Design and Mechanical of an Integrated Reflectometry System Module for the DEMO Project

Luís Manuel Carreira Prior

luis.prior@tecnico.ulisboa.pt

Instituto Superior Técnico, Universidade de Lisboa, Portugal

June 2018

Abstract

A conceptual development of an integrated reflectometry system module for the DEMO project is presented. Motivation arises from the fact that the modules, made of Eurofer97, are subjected to high thermal loads resulting in surface temperatures of the modules greater than 1300℃, well above the maximum material operating temperature of 550℃. Hence, it is necessary to develop a cooling system capable of maintaining the temperatures of the module less than 550℃, while complying with the DEMO nuclear fusion requirements. The work here presented contemplates a conceptual development for the reflectometry module and its cooling system recurring to CAD models and thermo-structural finite element analyses. With this, a conceptual model is proposed presenting a modulus surface temperature reduction of about 70% and a maximum module temperature of 20% below the maximum material operating temperature. At structural level, the thermal displacements are determined to be less than 0.5% of the deformed length. The stresses obtained are compared with the tensile yield stresses of the materials, being overall below the reference values. Lastly, a manufacturing methodology of the module, based on the manufacturing processes used in the Breeding Blanket, is proposed. For further work it is suggested a more detailed contact study of the module regarding the fixation systems as well as the manufacturing methods of the components.

Keywords: DEMO, Reflectometry, Nuclear Fusion, Finite Elements, Thermal-structural analysis

1. Introduction

Nowadays, energy is the central axis of modern civilization's life and economic growth.

To meet the increasing energy demand, which according to the International Energy Agency's 2016 data [1], is expected to be more than 30% by 2040, and to reduce greenhouse gas emissions, it is necessary to discover new sources of energy capable of replacing fossil fuels.

In this sense, nuclear fusion energy has been considered as a new energy resource of enormous potential and value to be exploited as it presents several advantages over traditional resources as well as sustainable, economic, safe and clean characteristics. Hence, nuclear fusion has promising prospects for growth to be the energy of the future.

One of the methods of achieving nuclear fusion on Earth is the magnetic confinement of plasma in specific devices, of which the Tokamak [2] stands out.

The ITER tokamak, currently been built in Cadarache (south of France) is expected to be the first nuclear fusion reactor capable of producing energy with an efficiency greater than 1, actually approximately 10.

The DEMO project, also based on the Tokamak for plasma confinement, is expected to the last step before the commercialization of electricity from nuclear fusion. The core requirements for DEMO focus on its ability to generate 500 MW net of electricity to the grid and operate on a closed-loop fuel cycle, i.e. produce and burn tritium in a closed loop.

One of the challenges in developing a Tokamak for power generation is to ensure constant operation, and for it is essential to ensure that the plasma remains confined without touching the inner surface of the Tokamak. The determination of plasma positioning can be done with electromagnetic diagnostics, which present a relatively higher error at elevated temperatures, or by reflectometry systems.

Reflectometry systems enable the relative position of the plasma in the vacuum chamber of a nuclear fusion reactor to be determined more accurately and with higher reliably during steady state operation.

This work presents the conceptual development of an integrated reflectometry system to be integrated

into the DEMO project. The concept presented in this work is based on an independent structure of a cassette module, here designated as Slim Cassette (SC), see Figure 1, that contemplates antennas, waveguides (WG), and cooling circuits. It is here approached from the feasibility point of view of an independent cassette module, which is to be positioned inside the Tokamak, as a complete blanket module, occupying a toroidal section with a thickness of approximately 200 mm. It will be subject to high thermal loads, derived from thermal radiation and ionizing radiation and therefore provided with an active pressurized helium cooling system.

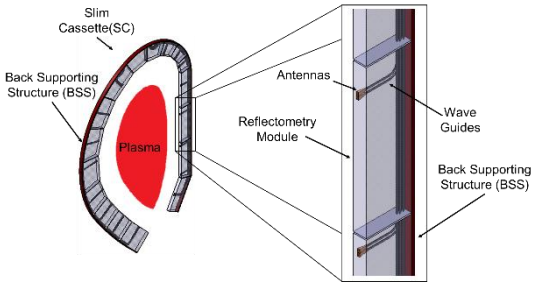

Figure 1 - Summary description of diagnostic module components

Initially, a CAD model of a reflectometry module with an integrated cooling system is developed. Afterwards, it is subject to Finite Element (FE) discretization and steady state FE thermal analyses. These thermal FE analyses of the cooling system are conducted to aid and support the improvement of the conceptual module. Subsequently, structural FE analyses of the conceptual module are conducted for characterization of the mechanical response of the module due to the plasma thermal loads. Concluding, a brief insight on possible manufacturing processes for the diagnostics module is provided.

The results obtained via thermal FE analyses are conclusive, i.e. the cooling requirements are verified with a reduction of about 70% of the surface temperature leading to a maximum temperature of the reflectometry module 20% below the maximum material operating temperature.

Following, are presented the fundaments that support this study, the methodologies adopted, the results and respective discussion and to conclude some final remarks are provided.

2. Fundaments

2.1. Fundaments of Heat transfer

Provided that a temperature gradient exists, heat transfer occurs, in three modes: conduction; convection, and radiation.

For a 1-D isotropic medium, the heat flux q''_{cond} may be expressed by Fourier's law [3] as

$$q''_{cond} = -k\,\frac{\mathrm{dT}}{\mathrm{dx}}, \tag{1}$$

where T and k are the temperature distribution and the thermal conductivity of the medium, respectively.

The convective heat flux q''_{conv}, may be expressed by Newton's law of cooling [3] as

$$q''_{conv} = h(T_s - T_\infty), \tag{2}$$

where T_s and T_∞ are the surface and fluid temperatures, respectively and h is the convective coefficient. Note that h depends on the type of convection (natural or forced) and fluid flow (internal or external), among others.

The Reynolds' number Re_D for forced convection in internal flow, may be expressed [3] as

$$Re_D = \frac{\rho u_m D_h}{\mu} = \frac{\dot{m} D_h}{A\mu}, \tag{3}$$

where ρ is the material density, u_m is the mean flow velocity, μ is the viscosity of the fluid, $\dot{m}$ is the mass flow rate, A is the internal cross-section area of the channel and D_h is its characteristic hydraulic diameter that may be expressed [3] as

$$D_h = \frac{4A}{P}, \tag{4}$$

where P is the internal perimeter.

For a circular tube with a uniform surface heat flux and laminar, fully developed conditions, the Nusselt number Nu_D may be assumed as a constant, independent of ReD, Pr, and axial location and Nu_D may expressed [3] as

$$Nu_D = h\,D_h/k. \tag{5}$$

For turbulent and fully developed flow (where $Re_D \geq 10^3$ and Pr between 0.6 and 160) then,

$$Nu_D = 0{,}023\,Re_D^{4/5}\,Pr^n, \tag{6}$$

where, n is 0.4 if $T_s > T_m$ and 0.3 if $T_s < T_m$ and T_m is the mean fluid temperature.

Concerning radiation, the net rate of radiation heat transfer flux $q"_{rad}$ may be expressed [3] as

$$q"_{rad} = \varepsilon\sigma(T_s^4 - T_{sur}^4). \tag{7}$$

Considering that the heat exchange occurs between a small surface at T_s and a larger isothermal surrounding gray or black surfaces at T_{sur}, where ε is

the emissivity of the surface of the body ($0 \leq \varepsilon \leq 1$) and σ is the Stefan-Boltzmann constant.

Note that solving radiation problems recurring to computational methods, require the estimation of the view factors that may be performed using the hemicube method [4].

Internal heat generation, due to the neutrons collisions with the atoms of a body may be estimated using the Monte Carlo N-Particle (MCNP) code in which the energy deposition F_6 may be expressed as

$$F_6 = \frac{\rho_a}{V\rho}\int_V \int_t \int_E \sigma_t(E_{par})H(E_{par})\varphi(r_s, E_{par}, t)dE_{par}\,dtdV\,, \quad (8)$$

where t is the discharge time, V is the volume of material, ρ_a is the atomic density, ρ is the density of material, $\varphi(r_s, E, t)$ is the particle flow, $H(E_{par})$ is the heating response and $\sigma_t(E_{par})$ is the microscopic total cross-section [5].

The internal heat generation may then be estimated by multiply F_6 by the intensity of the source of particles (source of neutrons) and by the density of the material.

2.2. Fundaments of Thermoelasticity

An isotropic body that is subjected to a temperature higher than its equilibrium temperature T_0, is likely to suffer body deformations by means of thermal expansion. This temperature difference ΔT will generate thermal stresses and thermal strains which according to Hooke's law can be expressed as:

$$\{\sigma\} = [E]\{\varepsilon^e\}\,, \quad (9)$$

where $[E]$ is the elastic properties matrix, $\{\sigma\} = \{\sigma_x\ \sigma_y\ \sigma_z\ \tau_{xy}\ \tau_{yz}\ \tau_{zx}\}$ the stress vector and $\{\varepsilon^e\}$ is the elastic strain vector for small deformations expressed as:

$$\{\varepsilon^e\} = \{\varepsilon\} - \{\varepsilon^t\}\,. \quad (10)$$

where

$$\{\varepsilon^t\} = \{\alpha T\ \alpha T\ \alpha T\ 0\ 0\ 0\}\,, \quad (11)$$

where α is the thermal expansion coefficient and T is the temperature of the element.

Assuming that both $[E]$ and α remain constant along the heating process Eq. (9) may be expressed as

$$\{\sigma^t\} = [E]\{\varepsilon^t\}\,, \quad (12)$$

where σ^t is the thermal stresses vector.

2.3. FEM Applied to Heat Transfer

A thermal FE analysis is governed by the heat transfer equation that can be expressed [6] as

$$\begin{gathered}[C]\{\dot{T}\} + [K_T]\{T\} = \{R_T\} \\ [K_T] = [K_c] + [K_h] + [K_r]\,, \\ \{R\} = \{R_T\} + \{R_c\} + \{R_h\} + \{R_r\} + \{R_{\dot{q}}\}\,,\end{gathered} \quad (13)$$

In Eq. (13) consider that, $[C]$ and $[K_T]$ are the global specific heat and thermal conductivity matrices, $\{R_T\}$, $\{T\}$ and $\{\dot{T}\}$ are the global thermal load, temperature, and the first derivative of the temperature vectors, respectively. Also, $[K_k]$, $[K_h]$ and $[K_r]$ are the global matrices of conduction, convection, and radiation, and $\{R_T\}$, $\{R_c\}$, $\{R_h\}$, $\{R_r\}$ and $\{R_{\dot{q}}\}$ are the global heat flow, convetion, radiation and heat generation vectors, respectively.

The FE analysis is performed using commercial software ANSYS® established as nonlinear thermal analysis (as radiation is considered and the properties of the materials are temperature dependent) that considers conduction, radiation and convection effects.

2.4. FEM Applied to Structural Analysis

Regarding the elasticity field, a few other components must be considered. This way the following equation must be considered:

$$[K]\{q\} = \{f\} = \{p\} + \{h\}\,, \quad (14)$$

where $[K]$ is the element stiffness matrix, $\{h\}$ is the thermal vector and $\{p\}$ is the forces vector, where each takes the following forms:

$$[K] = \int_V [B]^T[E][B]dV\,. \quad (15)$$

The global equation system may be represented by Eq. (17), where $[K]$ is the elasticity matrix, $\{Q\}$, the displacements vector and $\{F\}$, the force vector:

$$[K]\{Q\} = \{F\}\,. \quad (16)$$

The global matrixes and vectors are the result of a specific arrangement of matrixes and vectors of each element and is dependent on the spatial discretization. The problem can be solved both through iterative and direct methods, depending on its complexity. The direct methods are faster and accurate for simple systems, for complex systems the iterative method presents a good approximation.

3. Methodology

For the conceptual design of the reflectometry module, the methodology illustrated in Figure 2 is developed and implemented.

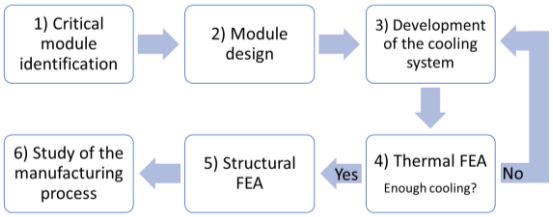

Figure 2 - General methodology adopted for the conceptual design of the reflectometry module

Before proceeding to the FE analyses of the module, three verification models (convection, radiation and thermoelastic) are introduced to verify (by comparing the numerical and analytical solutions obtained) the implementation of the fundamental concepts and tools.

3.1. Verification Models

The first verification model refers to heat transfer by convection in which is considered a parallelepiped, as shown in Figure 3, of length L, square side section a and with a hole of diameter D along the entire length. A flow q'', is imposed on one side of the body while the remaining faces are considered adiabatic. Additionally, a flow of a fluid with mass flow $\dot{m}$, mean inlet temperature $T_{m,i}$ and average outlet temperature $T_{m,o}$ is considered along the hole:

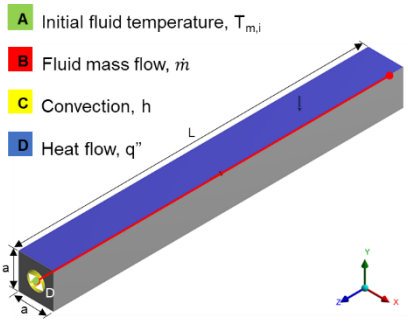

Figure 3 - Geometry and boundary conditions for the convective verification model

The objective is to estimate the outlet temperature, $T_{m,o}$, of the fluid as well as the average hole surface temperature $T_{m,s}$.

The second verification model focuses on heat transfer by thermal radiation and consists on determining the heat exchanges by radiation between two surfaces at different temperatures. For it are consider two irradiating surfaces with temperatures, T_1 and T_2, and emissivity, ε_1 and ε_2, spaced by a distance L, at an environment temperature T_a, see Figure 4.

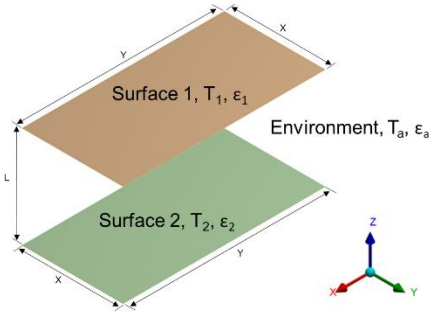

Figure 4 – Radiation verification model

In this case, the objective is to assess the accuracy of ANSYS® shape factor and radiosity solver calculations.

The thermoelastic model consists of a fixed square beam of length L subject to a temperature gradient $\Delta T = T - T_i$, as shown in Figure 5, and is here considered to verify the implementation of the theoretical concepts in the numerical calculation of displacements and stresses resulting from the thermal expansion of the model that is subject to a thermal gradient.

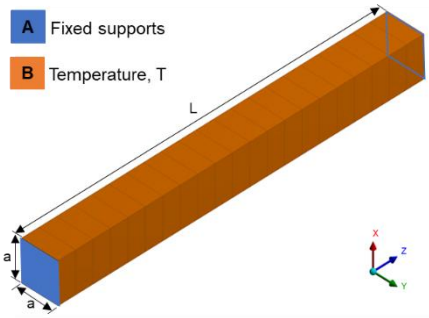

Figure 5 - Thermoelastic verification model

Once successful verification of the models is achieved, the critical module identification follows.

3.2. Critical Module Identification

To identify the critical module, thermal FE analyses of a body irradiating a flux Q to the surfaces of the seventeen modules are conducted to simulate the radiative heat exchange between the plasma and SC.

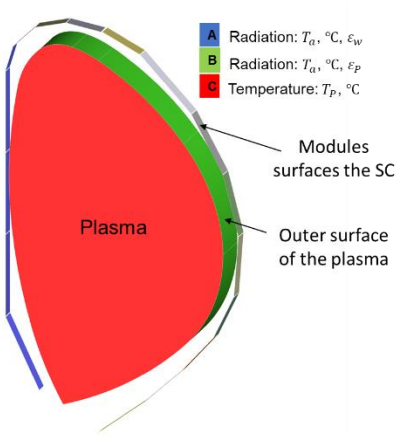

Figure 6 - Configuration used in critical module analysis

For it, three conditions are applied to simulate the plasma radiative flux, see Figure 6. Condition A and B simulate the surface to surface radiation exchange between the outer surface of the plasma and the inner surfaces of the SC, in an environment at a mean temperature, T_a, and whose emissivities of the surfaces are, respectively, ε_P and ε_W. Condition C sets the temperature of the plasma so that it emits a radiative flux Q according to the requirements established for DEMO.

3.3. Module Design

The implementation of the DEMO reflectometry system requires the antennas be placed in front of the plasma. Consequently they are considered to be made of Eurofer97 with additional W coating or entirely made of W. The WG, are also assumed to be made of Eurofer97, and must be routed from the antennas up to the diagnostic hall (see, Figure 7 b)).

This implementation concept is based on the development of a dedicated dummy section of the Body Blanket (BB) module. The SC is independent dummy sector (2x half-full poloidal sector) and is attached to the Back Support Structure (BSS), see Figure 7 a).

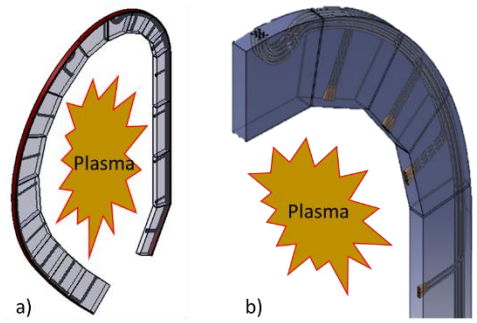

Figure 7 - SC independent: a) dummy section attached to the BSS; b) half-full poloidal sector

Even though several options are still being discussed regarding the sharing of the first wall (FW) and the common BSS between the BB and the SC module, the concept presented in this work is based on the independent SC structure with independent FW as illustrated by Figure 8 b).

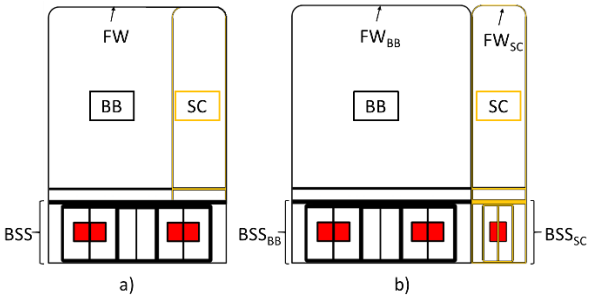

Figure 8 - Illustration of two possible attachments: a) common BSS -the SC is fixed to the front of the BSS and; b) independent SC sector - the SC is attached to the side of BSS

Hence, the design concept here developed assumes the same boundary conditions as those for the BB modules. As the SC is attached to a common BSS it is not desirable that thermal stresses arise between. Additionally, the mass density of the SC must be similar to the BB average mass density and a double barrier arrangement has to be employed to assure that the He coolant fluid will be contained. Furthermore, an equivalent shielding function to that of the BB should to be provided.

In this study a conceptual design of the critical module of the SC is developed, see Figure 9, by means of the CATIA V5® software.

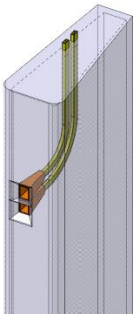

Figure 9 - Integration of antennas and WG on the critical module

Note that it is necessary to meet several design requirements imposed by the position of the module and the components that surround it, e.g., width and depth of the module, antennas and WG dimensions [8], among others.

3.4. Cooling System Development

As the reflectometry module is one of the plasma facing components, the existence of a cooling system in the module becomes indispensable to obtain the

required conditions that allow for the correct functioning of the diagnostic mechanisms.

Thus, a first conceptual design of the cooling system of the module is developed in which minimal changes are considered in order to maintain the constitution of the reflectometry module similar to that of the BB. The refrigeration system is based on high-pressure helium channels developed along the entire FW. Due to the need to remove heat from the interior of the module, two vertical cooling sections are additionally developed as a complement to the FW cooling.

To further improve the cooling capacity of the system, a second conceptual design is developed. Note that it is required to maintain the maximum temperatures of the module bellow the required operational temperature of 550^0C. For it, the vertical cooling sections are withdrawn and additional cooling channels are added to the inner blocks and distributed along the entire height of the module in a similar way to the channels of the FW. The assembly of these inner blocks channels with the FW channels are illustrated in Figure 10.

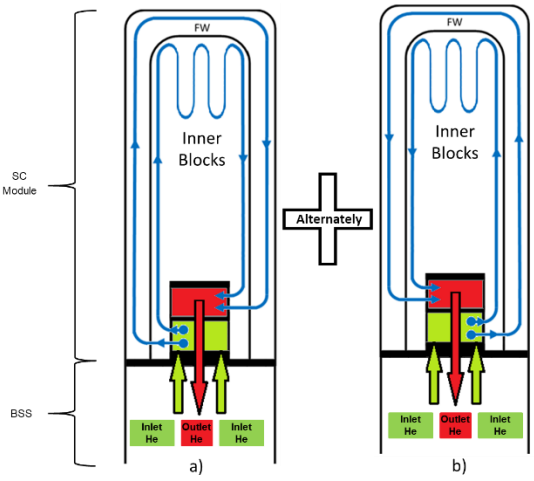

Figure 10 - Layout of which section with inner blocks cooling channels and FW channels: a) Horizontal odd sections; b) Horizontal even sections

To establish a double confinement barrier, *He* cooling pipes are implanted inside the cooling channels to form the first barrier while the second barrier is established by the assembly of the following section that functions as a cover plate to the previous one. The cooling channels are square section and their geometry is illustrated in Figure 11.

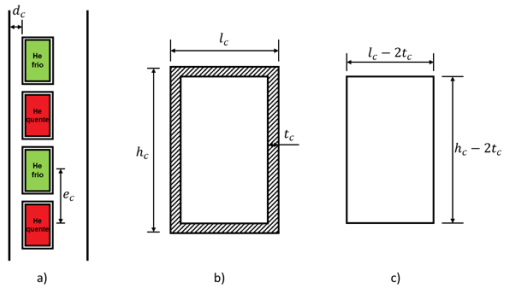

Figure 11 – Cooling channels: a) Channels distribution; b) He tubes geometry; c) He channel geometry

Another feature of the second conceptual cooling system design consists on the implementation of the cooling channels with the same geometry, as that illustrated by Figure 3.18, at the top and bottom of the module.

To further improve the cooling of the antennas, the distribution of the cooling channels in their surroundings are optimized in a way that they follow the geometry of the antenna.

3.5. Steady State Thermal FE Analysis

The CAD model developed for the reflectometry module with the cooling system is imported from CATIA V5®, simplified in ANSYS SpaceClaim and then directly used in the thermal FE analyses without further modifications.

The plasma and stray radiation heat fluxes [10], in ANSYS in ANSYS® are modelled as a radiating surface, at a certain temperature, emitting the correspondent thermal radiation heat flux which, minimizes the computational effort required for the FE analyses. The plasma thermal radiation is defined as a surface-to-surface radiation with a power density of 500 kW/m^2.

Considering the radiation heat flux, the nuclear heat generation, the irradiation surface area, the material volume of the module, the inlet *He* temperature ($T_{f,i} = 300$℃) and the estimated the *He* outlet temperature ($T_{f,o} = 463$℃) based on previous FE analyses, a study to determine the required mass flow $\dot{m}$ is conducted.

The convection coefficient h, is established based on Eq. 5 for a *He* flow with an average temperature $T_{f,m}$~400℃ and pressure $p = 80\ bar$.

The nuclear heat loads estimated with MCNP [9] are imported as internal heat generation, to account for the energy deposition by neutrons and photons in the SC module components.

3.6. Static Structural FEA

For the static structural FE analyses, several tie rods are implemented at the back plate of the module for displacement constraints, that are not addressed in this work.

The thermal heat loads previously estimated are directly imported to the structural FE analyses to evaluate the corresponding displacements and associated stresses.

Note that gravitational acceleration is assumed on the module to account for the force due to its own weight.

4. Results and Discussions

The main results obtained, and respective discussion follows.

4.1. Verification Models

Three verification models (Convection, Radiation and Thermoelastic) are initially considered. Using the methodology described in §3.1 the numerical the results obtained are presented in Table 4.1, For the convection model, a maximum deviation of approximately $4{,}19\%$ for T_s is obtained.

Table 4.2 and For the radiation model the deviation obtained for is of 6,4%.

Table 4.3 for the convection, radiation and thermoelastic verification models, respectively.

Table 4.1 - Analytical and numerical $T_{m,o}$ and T_s for the heat transfer by convection verification model.

	Analytical	Numerical
$T_{m,o}$ (℃)	200,00	202,69
T_s (℃)	560,64	584,13

For the convection model, a maximum deviation of approximately $4{,}19\%$ for T_s is obtained.

Table 4.2 – Deviation Δ between analytical and numerical results for thermal radiation verification model.

	ΔF_{ij}	ΔE	ΔG	Δq_{net}
$Surface\ 1$	~12.55	0,04	1,22	0,27
$Surface\ 2$		0,11	5,54	6,44

For the radiation model the deviation obtained for is of 6,4%.

Table 4.3 - Analytical and numerical δ_T and σ for thermoelastic verification model.

	Analytical	Numerical
$\delta_T\ (mm)$	3,9	3,9
$\sigma\ (MPa)$	819	819

The deviations obtained for the displacement and stresses in the thermoelastic model are both "zero".

All models present satisfactory relatively low deviations values and are therefore considered validated.

4.2. Critical Module Identification

Using the methodology described in §3.2, , it is possible to identify the inner equatorial module is identified as the critical module, see Figure 12, as it presents the maximum temperature.

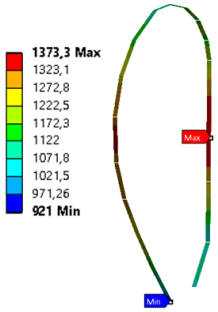

Figure 12 - Critical module identification

4.3. Module Design

The conceptual design of the module is developed following the methodology described in §3.3. Figure 13 illustrates the conceptual development process of the module.

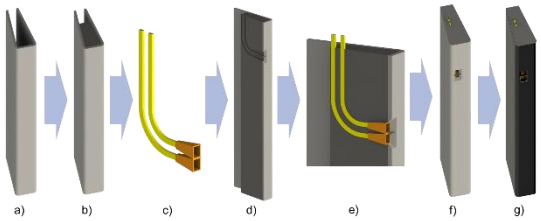

Figure 13 -Representation of the conceptual module development: a) Development of FW; b) Implementation of an inner block in the interior of the module; c) Modelling of antennas and WG; d) Groves for antennas and WG; e) Integration of the antennas and WG in the module; f) Cover plates of the tops of the module; g) Application of a tungsten cover on the front and sides of the module

4.4. Cooling System Development

Using the methodology described in §3.4 is used to develop the conceptual cooling system of the reflectometry module, see Figure 14.

The cooling system developed is constituted by square section channels in the FW and inner blocks at the top and bottom plates. All the channels are connected by two manifolds: Inlet manifold and Outlet manifold. The channels that supply the manifolds (see Figure 14 c) are only representatives as the connections to the BSS has not yet been decided.

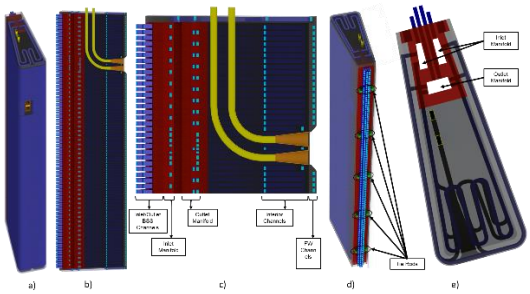

Figure 14 – Development of the final solution of the conceptual cooling system of the reflectometry module: a) Overview; b) Longitudinal cut; c) Identification of the different components of the system; d) Rear of the module; e) Top view

In Figure 14 it is possible to verify that the channels are distributed by levels along the vertical direction allowing manufacturability of the module using horizontal sections.

4.5. Steady State Thermal FEA

Steady state thermal FE analyses are conducted following the methodology described in §3.5.

It is assumed that the heat fluxes $q''_{rad} = 500\,\frac{KW}{m^2}$ may be approximated by a plasma radiating surface at a $T_s = 1450°C$, emitting similar thermal radiation heat flux which, minimizes the computational effort required by the subsequent analyses.

Based on the methodology described in §3.5, a mass flow $\dot{m} = 2{,}29\,\frac{Kg}{s}$ and a convection coefficient $h = 1959\,\frac{W}{m^2K}$ are determined analytically and used in the thermal FE analyses.

Additionally considering an initial temperature of the fluid of $T_{f,i} = 300°C$ and the nuclear heat loads imported from MCNP, the FEA is established.

The results obtained for the temperature on the reflectometry model are illustrated in Figure 15

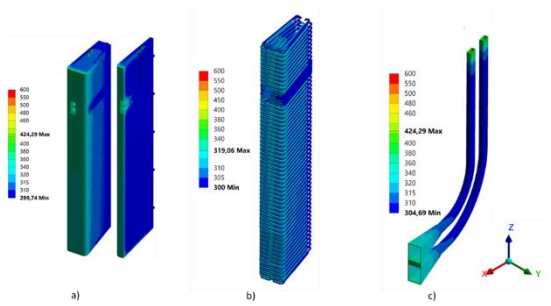

Figure 15 - Results obtained for the temperature of the 2nd conceptual cooling system design: a) inside and outside the module; b) in the cooling fluid; c) in the antennas and WG

Through an evaluation of the results obtained it is possible to verify that the hot spots detected in the first analysis [9] are not present, which in this sense validates the approach used to cool the upper and lower part of the module as well as the region of the antennas.

This is further supported by the fact that the maximum temperature obtained of $424{,}29°C$ is lower than the maximum operating temperature ($T_{max} = 550°C$) required. From Figure 15 a) it is still possible to deduce that the mean temperature in the module is below 400 °C and that the maximum temperature occurs at the end of the WG that is justified by the inexistence of nearby cooling.

4.6. Static Structural FEA

Following the methodology described in §3.6 the heat loads are imported from thermal FE analysis, the displacement supports are established and the gravitational acceleration is applied to all module mass.

Initially, an evaluation of the module displacements, see Figure 16, is conducted.

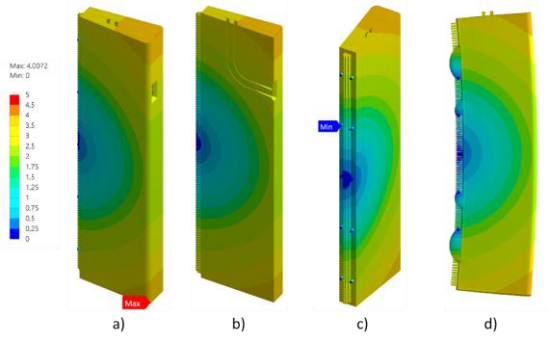

Figure 16 - Displacement [mm]: a) Overview; b) Interior of the module; c) Back of the module; d) Displacements (magnification 170x).

From the displacement results and based on the height of the module ($2300\,mm$) it is possibly to achieve that the maximum deformation is lower than 0,5% of the deformed length.

The results obtained for the vonMises stresses on the body of the reflectometry module (without W cover, antennas and WG) are illustrated in Figure 17.

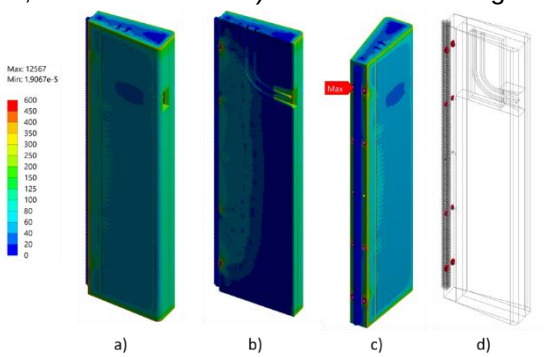

Figure 17 - Stress in Eurofer97 module in [MPa]: a) Overview; b) Interior of the module; c) Back of the module; d) Elements with a voltage greater than 600 MPa.

From Figure 17, one can verify that in general the stresses in the interior of module are below the elastic limit of the Eurofer97 ($450MPa$ for the maximum temperature achieved on the module $\mathrm{T} = 425℃$). Figure 17 c) shows that the maximum value ($\sim 12{,}6\ GPa$) obtained for the stress inside the module occurs in the region of the tie rods, from which one may conclude that it may not be the most appropriate and should be resized or altered in future work.

Regarding the antennas and WG, the stress results are illustrated by Figure 18

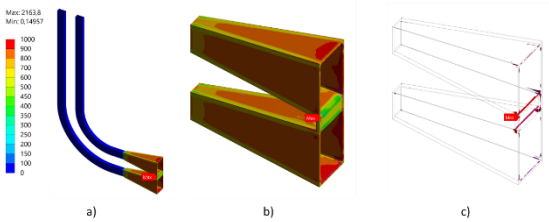

Figure 18 - Stress in antennas and WG [MPa]: a) Antennas and WG; b) Antennas; c) Elements with stress greater than 1000 MPa in the antennas.

As can be seen in Figure 18, the stresses in the WG (< 300 MPa) do not exceed the yield stress of Eurofer97 (~ 450 MPa at $\mathrm{T} = 425℃$) and present a maximum value in the antennas contact region which is a material transition modelled using a bonded contact. Higher stresses are present in the antennas, in the range of $900\ MPa$ and $1000\ MPa$. However, this is also the range of the tungsten yield stress values recorded for the antenna. In the Figure 18 c) it is possible to verify that only in very localized zones with relevant geometric transitions (edges), stress exceeds 1000 MPa.

4.7. Manufacturing Procedure

To approach the manufacturing procedure of the proposed conceptual design, the feasibility of the developed module is studied. It is decided to make some changes in the concept, of which the main one is the replacement of the concept of a module constituted by the FW and inner blocks by a concept based on a single block made from Eurofer97 and designated module body.

The cooling channels tubes and Wg made of Eurofer97 and the reflectometry antennas made of tungsten are incorporated in module body after which, the front and sides of the module body are covered with a 2 mm layer of tungsten.

With regard to the manufacture of the tubes of the cooling channels and according to [11] [6] it is suggested that they are manufactured using hot isostatic pressure (HIP). With it is possible to achieve the desired rectangular profiles with the required surface finishing and without compromising the mechanical properties of the material.

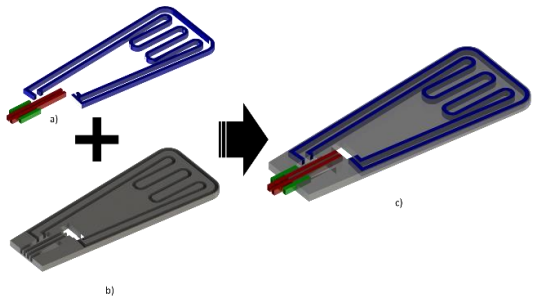

Figure 19 - Representation of the integration of the tubes into a generalist plate: a) Tubes already with defined geometry; b) Machined sheet c) Tubes integrated in the respective plate

Regarding the distribution of the channels along the height of the module (see Figure 11 and Figure 14 c)), it is suggested that the manufacture of the module body is to be made by sections that are consecutively coupled one after the other. The sections consist of Eurofer plates of constant thickness and machined to obtain the external shape of the module as illustrated by Figure 19 b). In each of the sections, the channels for the cooling tubes could be machined by milling. After machining each section, the respective tubes are inserted so that the upper face of the section is aligned with the upper face of the channel, as shown in Figure 19. At this point it is necessary to fix the tube to the plate. For that it is suggested the use laser welding as shown Figure 20.

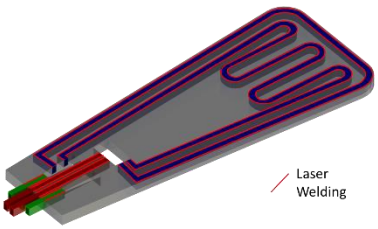

Figure 20 - Layout of the welding of the He pipes to the corresponding plate

After fixing all the cooling tubes to the respective plates, the module body assembly illustrated by Figure 21 starts. For the connection between the various sections it is suggested the use of the diffusion welding process, which consists of the simultaneous application of heat and pressure loads [11].

With this configuration, the requirement for the existence of a double barrier between the cooling circuit and the Tokamak interior is verified by placing

the tubes within the successive blocks with the application of the weldment.

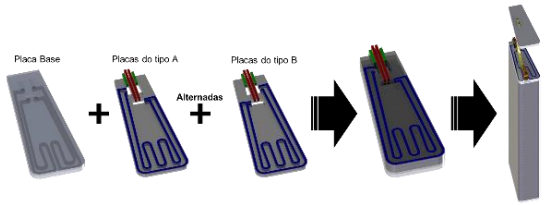

Figure 21 - Representation of the assembly process of the various sections of the interior of the module

To achieve this assembly, it will be necessary to develop a tool of the kind that allows to maintain the alignment of the plates throughout the assembly, as well as the correct positioning of the antennas and the WG, avoiding compromising their performance, they can be placed freely inside a "sleeve", guaranteeing the double barrier. An increase in the thickness of the waveguides may be necessary to reduce the stresses accumulated during the welding processes.

At the end of the section assembly, the side and front surfaces are polished, and the tungsten cover is added, closing the module assembly.

5. Conclusions

With the objective of not exceeding the maximum service temperature of $550℃$, different CAD models are developed, of which two are studied thermally and one structurally through finite element analysis using the commercial software ANSYS®.

In this work, FEA are performed on two concepts of cooling system. The first allows to conclude that the first concept for the developed cooling system is not sufficient, requires localized cooling in the upper and lower parts as well as in the region of the antennas. Additionally, it is concluded that the module needs a greater cooling inside, in order to reduce the impact of the internal heat generated by the ionizing radiation.

A second cooling system concept and its thermal FEA allow to validate the system, having a mean surface temperature reduction of the modulus of about 70% for $T_s = 400℃$ and a maximum temperature in the module $(424{,}29℃)$, 20% lower than the maximum material operating temperature $T_{max} = 550℃$. The structural FEA performed to this conceptual model based on the temperatures obtained from the thermal FEA allows to evaluate the mechanical behaviour of the developed module. It is possible to conclude that, in general the stresses in the module due to the thermal loads (in tungsten $\sim 900\ MPa$ and Eurofer97 $\sim 100\ MPa$) are lower than the elasticity limits of the materials of the module components (in tungsten $\sim 1000\ MPa$ and Eurofer97 $\sim 450\ MPa$). However, it is possible to verify that direct transitions from Eurofer97 to tungsten generate stress concentrations and, for this reason, should be avoided or otherwise improved the contact between both.

Acknowledgments

I would like to acknowledge my supervisors Eng. Paulo Quental, Doctor Hugo Policarpo and Professor Artur Malaquias, my family and my friends for all the support provided.

References

[1] I. Energy Agency, «International Energy Agency, Together Secure Sustainable Executive Summary», 2016.

[2] Y. Song, W. Wu, and S. Du, «Tokamak engineering mechanics», Springer-Verlag Berlin Heidelberg 2014.

[3] F. P. Incropera and D. P. DeWitt, «Fundamentals of Heat and Mass Transfer», Water, vol. 6th. p. 997, 2002.

[4] ANSYS, «Theory Reference for the Mechanical APDL and Mechanical Applications», Knowl. Creat. Diffus. Util., vol. 3304, April, pp. 724–746, 2009.

[5] R. Santos et al., «Material assessment for ITER's collective Thomson Scattering first mirror», 2015 4th Int. Conf. Adv. Nucl. Instrum. Meas. Methods their Appl. ANIMMA 2015, April, pp. 2–6, 2015.

[6] G. P. Nikishkov, «Introduction to the Finite Element Method» 2009 Lecture Notes. University of Aizu, Aizu-Wakamatsu 965-8580, Japan.

[7] Ansys, «ANSYS Elements Reference», August, 2005.

[8] N. C. Luhmann Jr., H. Bindslev, H. Park, J. Sánchez, G. Taylor & C. X. Yu «Chapter 3: Microwave Diagnostics», Fusion Science and Technology, 53:2, 335-396 (2008).

[9] R. Luís , R. Moutinho, L. Prior, P. B. Quental, A. Lopes, H. Policarpo, N. Velez, A. Vale, A. Silva, and A. Malaquias, «Nuclear and Thermal Analysis of a Reflectometry Diagnostics Concept for DEMO», IEEE Trans. Plasma Sci., pp. 1–7, 2018.

[10] P. B. Quental, H. Policarpo, R. Luís, e P. Varela, «Thermal analysis of the in-vessel components of the ITER plasma-position reflectometry», Rev. Sci. Instrum., vol. 87, n. 11, p. 11E720, Nov. 2016.

[11] A. Cardella et al., «The manufacturing technologies of the European breeding blankets», em Journal of Nuclear Materials, 2004.